Journal of Hazardous Materials 460 (2023) 132457

Contents lists available at ScienceDirect

Journal of Hazardous Materials

journal homepage: www.elsevier.com/locate/jhazmat

Research Paper

The divergent effects of nitrate and ammonium application on mercury methylation, demethylation, and reduction in flooded paddy slurries

Ji Chen [a,b,1], Gongren Hu [a,1], Jiang Liu [b,1], Alexandre J. Poulain [c], Qiang Pu [b], Rong Huang [d], Bo Meng [b,*], Xinbin Feng [b]

[a] College of Chemical Engineering, Huaqiao University, Xiamen 361021, China
[b] State Key Laboratory of Environmental Geochemistry, Institute of Geochemistry, Chinese Academy of Sciences, Guiyang 550081, China
[c] Biology Department, University of Ottawa, 30 Marie Curie, Ottawa, ON K1N 6N5, Canada
[d] College of Resources, Sichuan Agricultural University, Chengdu 611130, China

HIGHLIGHTS

- Different N fertilizations significantly influenced Hg transformation in flooded paddy slurries.
- NO_3^- inhibited both Hg^{II} methylation and MeHg demethylation.
- NO_3^- inhibited Hg^{II} reduction but NH_4^+ promoted Hg^{II} reduction.

GRAPHICAL ABSTRACT

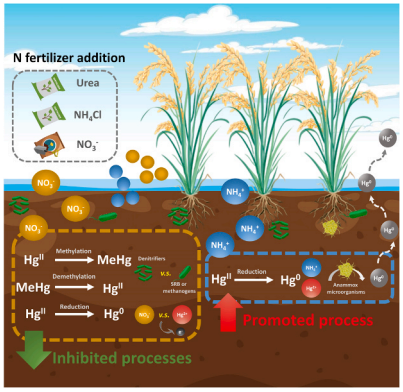

ARTICLE INFO

Editor: Edward Burton

Keywords:
Mercury transformation
Nitrogen fertilization
Flooded paddy soil
Multicompound specific isotope labeling

ABSTRACT

The production of methylmercury (MeHg) in flooded paddy fields determines its accumulation in rice grains; this, in turn, results in MeHg exposure risks for not only rice-eating humans but also wildlife. Nitrogen (N) fertilizers have been widely applied in rice cultivation fields to supply essential nutrients. However, the effects of N fertilizer addition on mercury (Hg) transformations are not unclear. This limits our understanding of MeHg formation in rice paddy ecosystems. In this study, we spiked three Hg tracers ($^{200}Hg^{II}$, $Me^{198}Hg$, and $^{202}Hg^{0}$) in paddy slurries fertilized with urea, ammonium, and nitrate. The influences of N fertilization on Hg methylation, demethylation, and reduction and the underlying mechanisms were elucidated. The results revealed that dissimilatory nitrate reduction was the dominant process in the incubated paddy slurries. Nitrate addition inhibited Hg^{II} reduction, Hg^{II} methylation, and MeHg demethylation. Competition between nitrates and other electron acceptors (e.g., Hg^{II}, sulfate, or carbon dioxide) under dark conditions was the mechanism underlying nitrate-regulated Hg transformation. Ammonium and urea additions promoted Hg^{II} reduction, and anaerobic

* Corresponding author.
E-mail address: mengbo@vip.skleg.cn (B. Meng).
[1] J.C., G.H., and J.L. contributed equally to this work.

https://doi.org/10.1016/j.jhazmat.2023.132457
Received 28 April 2023; Received in revised form 30 July 2023; Accepted 30 August 2023
Available online 1 September 2023

ammonium oxidation coupled with Hg^{II} reduction (Hgammox) was likely the reason. This work highlighted that nitrate addition not only inhibited Hg^{II} methylation but also reduced the demethylation of MeHg and therefore may generate more accumulation of MeHg in the incubated paddy slurries. Findings from this study link the biogeochemical cycling of N and Hg and provide crucial knowledge for assessing Hg risks in intermittently flooded wetland ecosystems.

1. Introduction

Human exposure to mercury (Hg) can have toxic effects on the nervous, digestive, and immune systems [10]. The organic form of Hg, methylmercury (MeHg), can bioaccumulate in biota and is then biomagnified along the food chain [78]. The consumption of fish has long been recognized as the predominant pathway underlying human exposure to MeHg [44,71]. However, studies of Hg-contaminated areas, where rice is the chief product, have indicated that rice consumption is the dominant MeHg exposure route, not only for local populations [14, 59,89] but also a global issue [31,42]. Follow-up studies have further confirmed that rice paddy fields, a typical artificial wetland, are a hotspot for the methylation of inorganic Hg (Hg^{II}) to MeHg [62,95,96], which then accumulates in rice grains during the rice-growing process [41,51–53,90]. Consequently, the investigation of Hg cycling mechanisms in rice paddy ecosystems has become a new challenge for scholars interested in the study of Hg. In particular, there remain gaps in our understanding of the microbiological and physicochemical mechanisms mediating the transformation of Hg species (Hg^{II}, MeHg, and elemental Hg^0) and their influences on net MeHg production in paddy fields.

Of all the nutrients required by rice, nitrogen (N) is usually deficient in paddy systems [37] because of pH-dependent ammonia volatilization and nitrification-denitrification processes [19]. In particular, rice is an ammonium-preference plant [33]. Due to the relatively low use efficiency of N (31–39%) in paddy fields [84,93] and to maintain rice yield in an intensified agricultural system, a large amount of N fertilizer is applied annually. For example, 29 Tg N yr^{-1} of N fertilizers were applied in 2010 globally [93], and 5.03 Tg yr^{-1} of N was applied in 2018 in China for rice cultivation [45]. In recent decades, the environmental consequences of N over-fertilization (e.g., eutrophication, greenhouse gas emissions, acidification, etc.) have been extensively studied. However, whether N fertilization influences Hg cycling in flooded paddy systems remains one of the least studied but important topics [67]. Moreover, different N fertilizers, including various N species (e.g., urea, ammonium, and nitrate), are used in agricultural fields [56], and different N fertilizers likely undergo different biogeochemical processes in paddy fields; examples include ammonia volatilization (from NH_4^+ to NH_3), nitrification (from NH_4^+ to NO_3^-), denitrification (from NO_3^- to N_2), dissimilatory nitrate reduction to ammonium (DNRA, from NO_3^- to NH_4^+), and anaerobic ammonia oxidation (from NH_4^+ to N_2), among others [26,30,63,97]. Therefore, to better understand the effect of N fertilization on Hg transformation in flooded paddy fields, different N species should be investigated; however, until now, this issue has been less considered.

Several existing studies have investigated the influences of different N species on Hg transformation in both agricultural and other ecosystems. For example, adding urea (NH_4^+ type N) enhanced not only the bioavailability of Hg but also the abundance of Hg-methylating microbes, which therefore promoted Hg methylation in paddy fields [70]. Moreover, [74,73,75] and Sun et al. [70] reported that long-term urea fertilization increases MeHg accumulation in rice (5.18–41.69%). Liu et al. [43] suggested that long-term N fertilization (inorganic N) reshapes the diversity of the *merA* gene, which influences Hg^{II} reduction indirectly. Li et al. [32] reported that adding NO_3^- will result in an imbalanced C, N, and S stoichiometric ratio, which will therefore shift Hg methylating communities and change the production of MeHg in paddy fields. In aquatic systems, research has documented that the presence of NO_3^- was found to significantly inhibit MeHg formation due to the competition between NO_3^- reducers and SO_4^{2-} reducers [13,50,65, 68,76]. Zhang et al. [88] reported that N_2O addition significantly inhibited MeHg formation in arctic tundra through the inhibition of sulfate-reducing bacteria (SRB). By spiking ^{14}C-enriched MeHg, Marvin-Dipasquale and Oremland (1998) successfully tracked the demethylation of MeHg in net MeHg formation (i.e., combined effects from Hg^{II} methylation and MeHg demethylation) and reported that MeHg demethylation was partially inhibited by NO_3^- addition in Everglades sediments. In addition to the competition between microbes that are involved in Hg methylation/demethylation and N cycling, *hgcAB* gene-harboring microbes have also been found to be involved in both denitrification and DNRA [67]. In the field of photochemistry, studies have revealed that NO_3^- can catalyze the photodegradation of MeHg [69] and the photooxidation of Hg^0 in surface waters [60]. Although some linkages between specific N species and Hg cycling have been documented, large knowledge gaps remain. Specifically, two major knowledge gaps require urgent attention. (i) The concurrent effects of N on the relative contributions of Hg^{II} methylation, MeHg demethylation, and Hg^{II} reduction to net MeHg formation. (ii) The roles of different N species (e.g., ammonium) in Hg transformation have seldom been reported and need to be determined.

To address the above knowledge gaps, we applied a multi-compound specific isotope labeling technique (i.e., spiking of $^{200}Hg^{II}$, $Me^{198}Hg$, and $^{202}Hg^0$ tracers) and different N fertilizers (i.e., urea, ammonium, and nitrate) to 3 paddy slurries with different Hg contamination gradients. The effects of different N fertilizers on Hg methylation, demethylation, and reduction were elucidated by tracking the isotopic signals of MeHg and purgeable Hg^0 tracers after N addition. The underlying biogeochemical mechanisms were revealed by combining isotopic, geochemical, and microbial approaches. This study addressed the following questions: (i) Can N species regulate Hg transformation in paddy slurries with different Hg concentrations? (ii) How do different N species regulate Hg transformation? Knowledge gained from this study will not only improve our understanding of Hg transformation in rice paddy ecosystems but will also contribute to our knowledge of the interplay between nutrients and Hg cycling in intermittently flooded environments.

2. Materials and methods

2.1. Sampling sites and sample collection

Three rice paddy fields with different Hg contamination gradients in Guizhou Province, Southwest China, were chosen for this study. The first site was located in a large-scale abandoned Hg mining region (site Sikeng, SK, E 109°12′38″, N 27°31′2″, [THg] = 609 ± 7 mg kg^{-1}), and the second site was in a small-scale preartisanal Hg smelting region (site Gouxi, GX, E 109°11′30″, N 27°33′50″, [THg] = 17.2 ± 1.7 mg kg^{-1}), both within the Wanshan Hg mining area. The third paddy field was a background control site located in a rural area ~30 km away from Guiyang City (site Huaxi, HX, E 106°31′28″, N 26°25‘20″, [THg] = 0.15 ± 0.003 mg kg^{-1}) [38]. Textures for the paddy soils at three sites are clay loam soil (HX: clay 34.0%, silt 33.0% and sand 33.0%; GX: clay 30.7%, silt 34.7% and sand 34.7%) and loam soil (SK: clay 15.3%, silt 36.7% and sand 48.0%) [39]. More background levels of Hg in the paddy fields of the study sites are shown in Table S1. It is worth mentioning that THg concentrations in contaminated paddy soils vary substantially among different paddy plots and even among different locations of the same plot, especially in this abandoned Hg mining

region [39,83]. Submerged soil samples (1–10 cm below the overlying water—soil interface) were collected and stored in precleaned 500 mL polypropylene (PP) bottles (Nalgene®, Thermo Fisher, USA) without any headspace. The corresponding overlying water samples (1–3 cm above the water—soil interface) were collected using acid-precleaned syringes and stored in PP bottles. All PP bottles were sealed with Parafilm®, double bagged, stored in a cooler with ice packs (~4 °C), and transported to the lab within 24 h. The sampling campaign was conducted on the 50th day after the transplantation of rice seedlings in 2019. This period was chosen because the methylation process was previously found to be active [95,96].

2.2. Incubation experiment

Anaerobic incubation using serum bottles (100 mL, borosilicate glass) was conducted in a glovebox (PLAS-LABS, USA). The paddy soils and overlying water were mixed to prepare incubation slurries with a moisture content of approximately 75% [38,39,83]. The homogenized paddy slurries (30 mL) were weighed in the incubation bottles, and the moisture content of each slurry was recorded. The treatments were as follows: urea ($CO(NH_2)_2$), ammonium chloride (NH_4Cl), and sodium nitrate ($NaNO_3$) addition treatments; autoclaved (121 °C for 30 min) treatment; and control treatment (without N addition). The same amount of N (equivalent to 200 mg N kg^{-1}) was added to the incubation bottles for the three N treatments based on the premeasurement of N species and the total N concentrations in the study paddy fields [58]. N species selected in this study are according to the statistical data from FAO [15]. Ammonium nitrate (NH_4NO_3) is a more widely used N fertilizer than $NaNO_3$ alone. However, it is very difficult to distinguish the influences of NH_4^+ and NO_3^- by using NH_4NO_3. Therefore, NH_4Cl and $NaNO_3$ were used in this study. All N species added in this study were at metals basis level (99.999%, Aladdin®, China). Three isotopically enriched Hg species (^{198}Hg 98.52 ± 0.15%, ^{200}Hg 98.09 ± 0.2%, and ^{202}Hg 98.68 ± 0.02%) were purchased from ISOFLEX (USA). Compound-specific Hg isotope tracers, including inorganic divalent Hg tracer ($^{200}Hg^{II}$), methyl-Hg tracer ($Me^{198}Hg$), and elemental Hg tracer ($^{202}Hg^0$), were synthesized and spiked into all incubation bottles. The preparation details for the Hg isotope tracers are provided in Text S1. The spiking dosage of each Hg tracer for each site is shown in Table S2. Typically, the spiking concentrations of Hg^{II} and MeHg tracers are 10% and 100% of the ambient concentrations, respectively [16,83,96]. Notably, the Hg^{II} tracers added in the incubation bottles using SK soil are only approximately 1% of ambient THg due to the extremely high ambient THg concentration ([THg] = 609 ± 7 mg kg^{-1}) [38]. All serum bottles were incubated in the dark (covered by aluminum foil) in a glovebox at room temperature (25 °C). Three random bottles from each site and each treatment were destructively sampled at 0 h, 12 h, 24 h, and 48 h. During the sampling processes, Hg^0 was first collected by purging the incubated slurries (argon gas, 300 mL min^{-1} for 20 min) and gold amalgamation; therefore, the Hg^0 determined in this study is recognized as purgeable Hg^0. It should be noted that the measured purgeable Hg^0 likely underestimates Hg^0 formation due to the presence of solid phase immobilization resulting in non-purgeable Hg^0 [34,38,81]. We assume that the solid phase immobilization for Hg^0 by using paddy soils from the same site is comparable. Therefore, the purgeable Hg^0 could still be used to represent Hg reduction at each site. The slurry samples used for isotopic MeHg species analysis were collected in 50 mL PP tubes (JET, BIOFIL, China) and then stored at − 20 °C after acidification by using 1 mL 6 N HCl to stop biotic reactions [17,38]. Due to the periods of incubation, bottle preparation, and subsampling, the actual time series for purgeable Hg^0 was 2 h, 14 h, 26 h, and 50 h, and for MeHg, it was 4 h, 18 h, 28 h, and 52 h. Samples used for DNA extraction were collected in 1.5 mL sterilized cryogenic tubes (Nalgene®, Thermo Fisher, USA) and stored at − 80 °C until further analysis. The remaining slurry samples were immediately centrifuged (RCF of 2850 g, 5 min, +4 °C) and filtered (0.45 μm PES filter, JIN TENG®, China); the isolated liquid phases were used to analyze the concentrations of N species (NH_4^+, NO_3^-, and NO_2^-), sulfate (SO_4^{2-}), sulfide (S(-II)), ferrous ion (Fe^{2+}), and ferric ion (Fe^{3+}). All of the incubation, isotope spiking, and subsampling procedures were conducted in an oxygen-free glovebox (PLAS-LABS, USA).

2.3. Analytical methods

Isotope-enriched Hg^0 ($^{198}Hg^0$, $^{200}Hg^0$, and $^{202}Hg^0$) and MeHg ($Me^{198}Hg$, $Me^{200}Hg$, and $Me^{202}Hg$) were measured using the external standard method [23,54]. Geochemical factors, including the concentrations of NO_3^-, NO_2^-, NH_4^+, SO_4^{2-}, HS^-, Fe^{2+}, and Fe^{3+}, were determined in the liquid phase of the paddy slurries. Quantitative PCR (qPCR) was employed using extracted slurry DNA. The abundances of functional genes associated with Hg and N transformation, including Hg methylation (*hgcA*), mercuric reductase (*merA*), organomercury lyase (*merB*), nitrate reductase (*narG*), nitrite reductase (*nirS*), and ammonia monooxygenase for ammonia-oxidizing archaea (AOA *amoA*) and bacteria (AOB *amoA*), were obtained (primers used in Table S3). The microbial communities were assessed using high-throughput sequencing of the 16 S rRNA gene amplicons for the V4-V5 regions with the primer pair 515 F (5′-GTGCCAGCMGCCGCGG-3′) and 907 R (5′-CCGTCAATTCMTTTRAGTTT-3′). More details on the measurements, DNA extraction, PCR conditions, sequencing, and qPCR are provided in Text S2.

2.4. Data analysis

Isotope-enriched Hg (^{198}Hg, ^{200}Hg, and ^{202}Hg) refers to Hg from the spiked tracers; this was calculated using a simplified approach based on the commonly used matrix-based signal deconvolution approach [61]. This approach was adopted due to the high purity of the prepared Hg isotope tracers [48,54]. The methylation rate constants (K_m-$^{200}Hg^{II}$ (d^{-1}) and K_m-$^{202}Hg^0$ (d^{-1})) and corresponding ratios of produced MeHg to spiked inorganic Hg tracers ($Me^{200}Hg/^{200}Hg^{II}$ (%) and $Me^{202}Hg/^{202}Hg^0$ (%)) were used to represent the methylation of spiked Hg tracers ($^{200}Hg^{II}$ and $^{202}Hg^0$). Similarly, the demethylation rate constant (K_d-$Me^{198}Hg$, d^{-1}) and the ratio of $Me^{198}Hg$ loss to spiked $Me^{198}Hg$ tracer ($Me^{198}Hg$ demethylation (%)) were used to represent the demethylation of spiked MeHg tracer ($Me^{198}Hg$). The volatilization rate constants (K_v-$Me^{198}Hg$ (d^{-1}) and K_v-$^{200}Hg^{II}$ (d^{-1})) and corresponding ratios of produced purgeable Hg^0 to spiked Hg tracers ($^{200}Hg^0/^{200}Hg^{2+}$ (%) and $^{198}Hg^0/Me^{198}Hg$ (%)) were used to represent the reduction of spiked Hg tracers ($Me^{198}Hg$ and $^{200}Hg^{II}$). Details for the calculations above are shown in Text S3 and in our parallel work [38]. Several assumptions were made in these calculations: (i) the methylation of Hg follows a pseudo-first-order rate law; (ii) the concentration of the products depends only on the concentration of the reactant but not on the other constituents in the system; (iii) the concentration of spiked Hg tracers at the beginning (t_0) remains approximately constant throughout the experiment; (iv) the rate of methylation of the Hg^{II} tracer exceeds the rate of demethylation of MeHg formed from the spiked Hg^{II}; and (v) the concentration of newly generated MeHg at the beginning (t_0) is zero [22,24,27,98].

2.5. QA/QC and statistics

The certified reference material (CRM) ERM-CC580 was used, and the recovery for the MeHg measurement of the CRM ranged from 76.2% to 108.4% with an average of 85.2 ± 9.07% (n = 26). Duplicates were added every 10 samples during measurement, and the relative standard deviation (RSD%) of duplicates was < 10%. The instrument detection limit for Hg using ICP—MS was 10 pg. Data are presented as the mean ± standard error (SE). The differences in data sets were assessed by t tests and one-way ANOVA with Duncan's post hoc test. All analyses were performed using SPSS 23.0 (IBM®, IL, USA). Statistical significance (p) was declared at < 0.05 (2-tailed).

3. Results

3.1. Variation in N species

Nitrogen species, including NO_3^-, NO_2^-, and NH_4^+, were measured. During incubation, the highest NO_3^- concentrations were observed in the autoclaved samples at sites GX (8.53 ± 0.77 mg L^{-1}) and SK (128.1 ± 7.11 mg L^{-1}) (Fig. 1). However, the NO_3^- concentrations in the other treatments were all extremely low (below 0.14 mg L^{-1}). Even in the $NaNO_3$ addition treatment, the NO_3^- concentration was below 0.23 mg L^{-1} (at the 4th and 16th hour for site GX). A decreasing trend in NO_3^- during incubation was detected in the $NaNO_3$ treatment at every site (Fig. 1). Similar to the distribution patterns of NO_3^-, the highest NO_2^- concentrations were observed in the autoclaved treatment at sites HX and GX. Moreover, there was no detectable NO_2^- in the NH_4Cl treatment at sites HX and GX or in all treatments at site SK (Fig. S1).

Ammonium was the dominant N species among NH_4^+, NO_3^-, and NO_2^- during the incubation process; the concentration of NH_4^+ was 1–2 orders of magnitude higher than that of NO_3^- at all sites ($p < 0.05$, Fig. 1 and Fig. S2). When grouping the NH_4^+ concentrations for each treatment across the different incubation periods, the NH_4^+ concentrations in the autoclaved, control, and $NaNO_3$ treatments were comparable ($p > 0.05$, Fig. S3) but were lower than those in the urea and NH_4Cl treatments ($p < 0.01$, Fig. S3). Furthermore, the NH_4^+ concentrations in the urea treatment were significantly higher than those in the NH_4Cl treatment at all sites ($p < 0.01$, Fig. S3).

3.2. Copies of the narG, nirS, AOA amoA, AOB amoA and hgcA genes

In addition to the concentrations of N species, functional genes related to N cycling were also considered (Fig. 2). At sites HX and SK, gene copies of denitrifiers (i.e., *narG*-encoded nitrate reductase and *nirS*-encoded nitrite reductase) steadily increased in the N addition treatments (urea, NH_4Cl, and $NaNO_3$ for site HX and urea for site SK) during

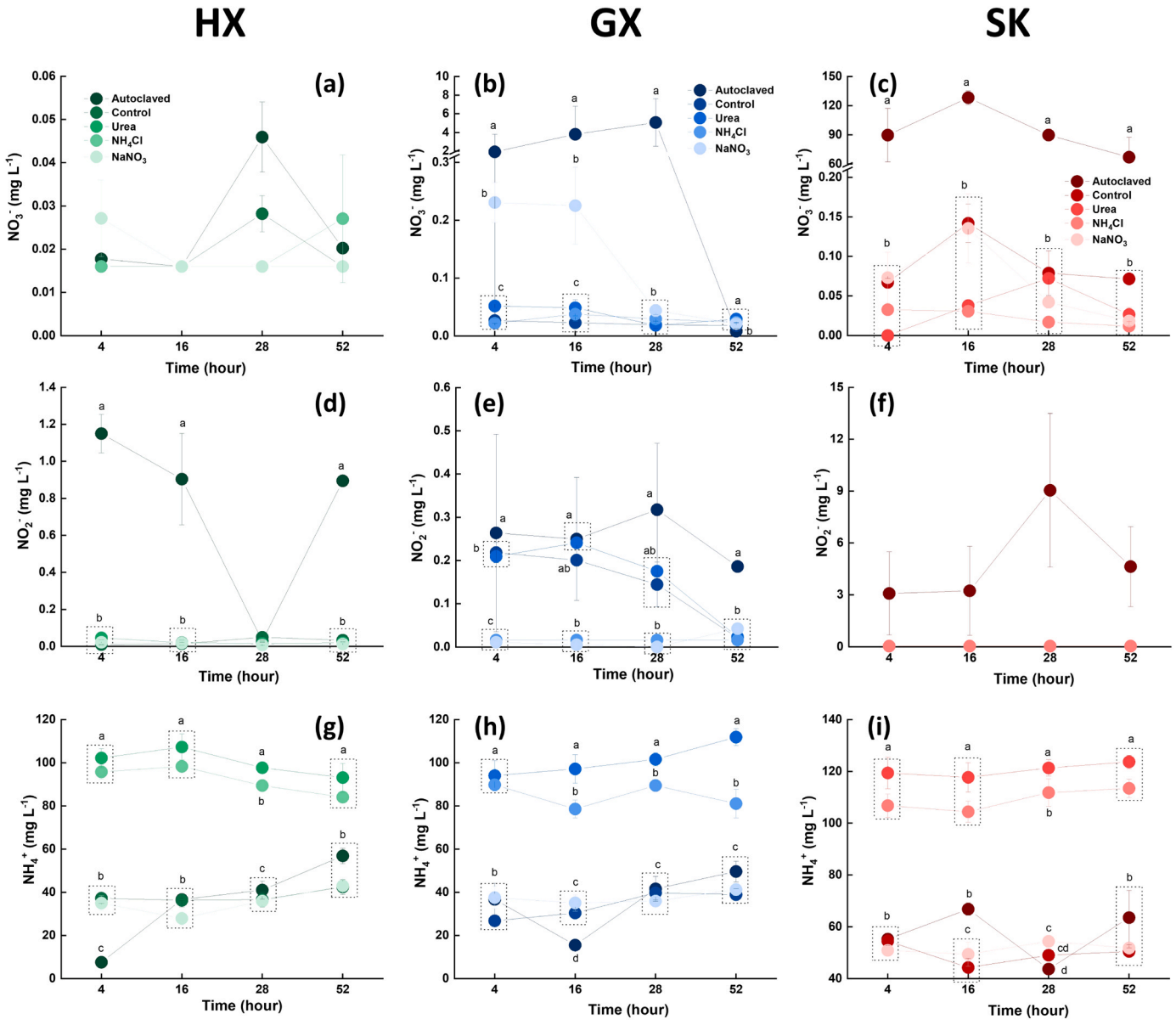

Fig. 1. Concentrations of NO_3^- (a-c), NO_2^- (d-f), and NH_4^+ (g-i) as a function of time at the three sites (HX, GX, and SK) for the different treatments. Error bars represent the standard error (± SE) of the replicates ($n = 3$). Different lowercase letters indicate that the differences among the treatments at the same incubation time are significant ($p < 0.05$). Data points in the same dashed line frame suggest an insignificant difference. Values below the detection limit were replaced by the detection limit value (NO_3^- and NO_2^- for 0.016 mg L^{-1}). Data on NO_3^- and NH_4^+ for the autoclaved and control treatments were obtained from our parallel work [38].

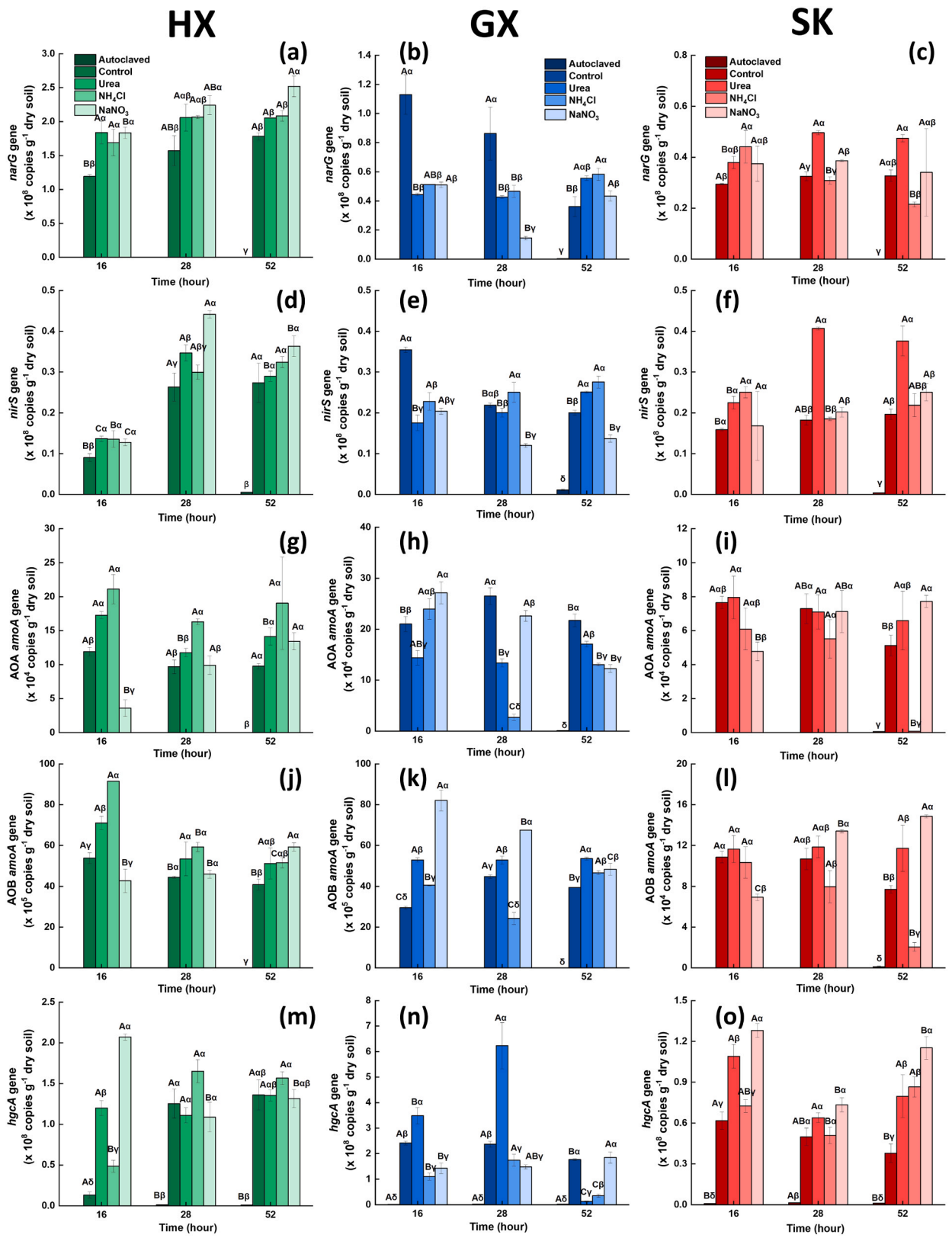

Fig. 2. Copies of *narG* (a-c), *nirS* (d-f), AOA *amoA* (g-i), AOB *amoA* (j-l), and *hgcA* (m-o) genes as a function of time at three sites (HX, GX, and SK) for different treatments. Error bars represent the standard error (± SE) for replicates ($n = 3$). Different Greek letters indicate that the differences among the treatments at each time point are significant (one-way ANOVA $p < 0.05$). Different capital letters indicate that the differences between the different time points for each treatment are significant (one-way ANOVA $p < 0.05$). Genes at the 4th hour were not determined. For N cycling-related genes in the autoclaved samples, genes were only determined at the 52nd hour.

the incubation period ($p < 0.05$, Fig. S4). Statistical analyses revealed significant positive correlations between the log(*narG*) and log(*nirS*) copies at all sites ($p < 0.01$, Fig. S5a).

The urea and NH_4Cl treatments significantly increased the *amoA* gene copies for both AOA and AOB at site HX ($p < 0.05$, Fig. S6). In addition, significant correlations between the *amoA* genes (both AOA and AOB) and NH_4^+ were observed at site HX ($p < 0.01$, Fig. S5b). However, similar trends in the NH_4^+ addition-regulated ammonia oxidation genes as above were absent at sites GX and SK (Fig. S6).

3.3. Redox of S and Fe

The redox conditions of S and Fe were revealed by the concentrations of SO_4^{2-}, HS^-, Fe^{3+}, and Fe^{2+}. Higher SO_4^{2-} concentrations were found in the autoclaved treatment at all sites when compared with the control and ammonium treatments ($p < 0.05$, Fig. S7). In addition, more SO_4^{2-} was observed in the $NaNO_3$ treatment than in the other treatments at sites GX and SK ($p < 0.01$; Fig. S7 and Fig. S8b and S8c). At site HX, however, the SO_4^{2-} concentration decreased within 16 h in the $NaNO_3$ treatment. At the end of the incubation period (the 52nd hour), higher HS^- was observed in the $NaNO_3$ and NH_4Cl treatments than in the control and urea treatments at site HX ($p < 0.05$, Fig. S7d), but this phenomenon was not observed at sites GX and SK.

Ferric ions (Fe^{3+}) were the dominant Fe species for all samples at site HX ($p < 0.05$, Fig. S8g), with the only exception being the autoclaved treatment, whereas Fe^{2+} was the major Fe species at sites GX and SK ($p < 0.05$, Fig. S8h and S8j). In the N treatments, high Fe^{3+} concentrations were sometimes observed in the $NaNO_3$ treatment (i.e., the 52nd hour at site HX and the 28th hour at site GX, $p < 0.05$, Fig. S7g and S7h). However, there were no significant differences in the Fe^{2+} concentration between the NO_3^- and NH_4^+ treatments at the end of the incubation period for all sites.

3.4. Microbial communities

A total of 8771,483 high-quality sequences were obtained and clustered into 18,370 OTUs. *Proteobacteria*, *Chloroflexi*, *Acidobacteria*, and *Actinobacteria* were the most abundant phyla (Fig. S9), and

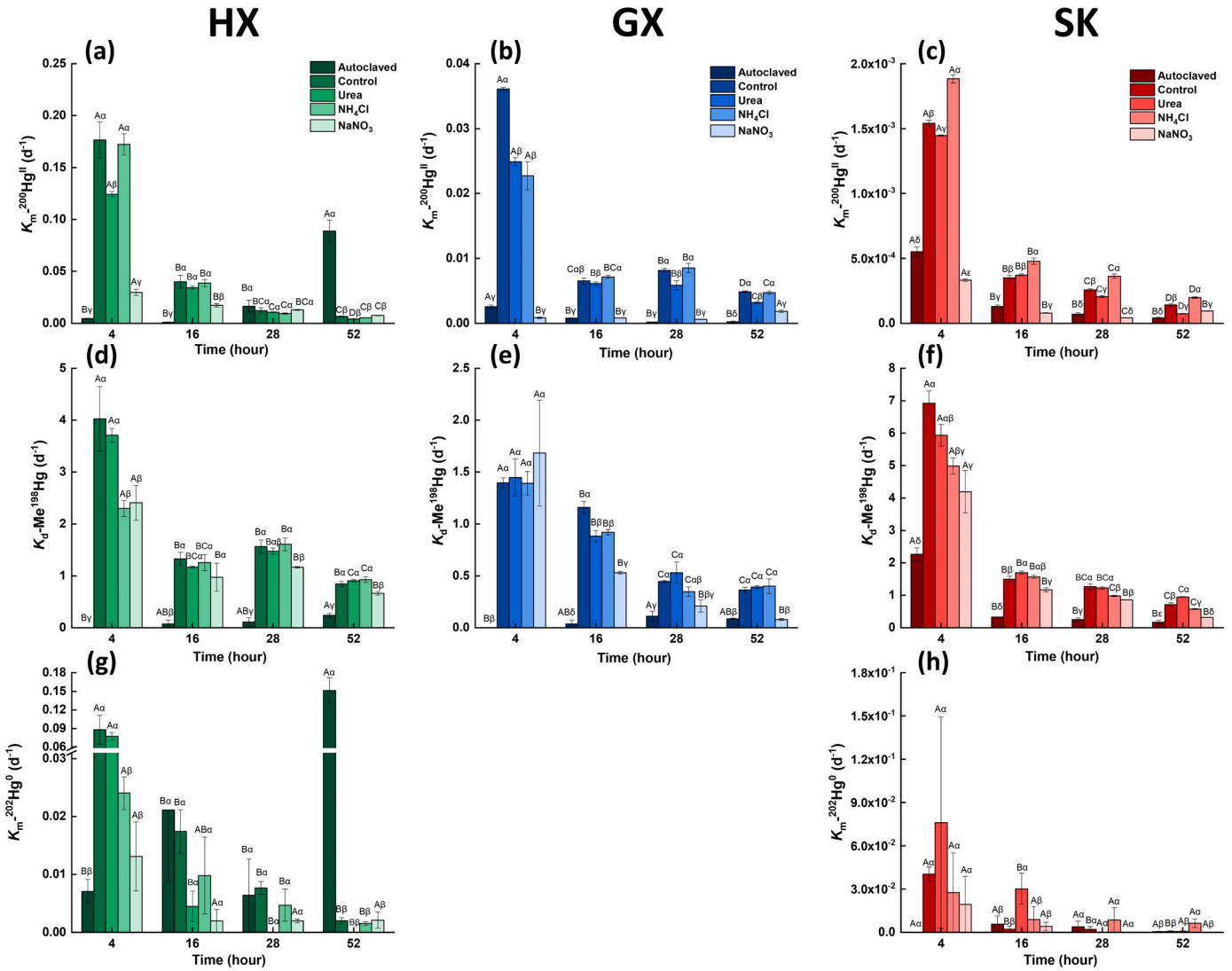

Fig. 3. Methylation and demethylation rate constants (K_m-$^{200}Hg^{II}$ in plots a, b, and c; K_d-$Me^{198}Hg$ in plots d, e, and f; and K_m-$^{202}Hg^0$ in plots g, and h) as a function of time at the three sites (HX, GX, and SK) for the different treatments. The formation of $Me^{202}Hg$ from spiked $^{202}Hg^0$ was not detected at site GX; therefore, the K_m-$^{202}Hg^0$ plot is not provided. The error bars represent the standard error (± SE) of the replicates ($n = 3$). Different Greek letters indicate that the differences among the treatments at each time point are significant (one-way ANOVA $p < 0.05$). Different capital letters indicate that the differences between the different time points for each treatment are significant (one-way ANOVA $p < 0.05$). The concentrations of $Me^{200}Hg$, $Me^{198}Hg$, and $Me^{202}Hg$ are shown in Fig. S11. Data for the autoclaved and control treatments were obtained from our parallel work [38].

significant differences in these phyla between the treatments were observed (Fig. S10). In addition, six genera of AOB or nitrite-oxidizing bacteria (*Nitrotoga*, *Thiocapsa*, *Nitrosospira*, *Nitrosomonas*, *Halomonas*, and *Nitrospira*), 15 genera of denitrifiers (*Sulfurifustis*, *Pseudomonas*, *Cupriavidus*, *Candidatus Accumulibacter*, *Candidatus Competibacter*, *Ahniella*, *Azoarcus*, *Halomonas*, *Dechloromonas*, *Rhodanobacter*, *Caballeronia Paraburkholderia*, *Prosthecomicrobium*, *Bradyrhizobium*, *Mesorhizobium*, and *Azospirillum*), and six genera of assimilatory nitrate reduction bacteria or DNRA (*Bacillus*, *Pseudomonas*, *Acinetobacter*, *Klebsiella*, *Clostridium*, and *Paenibacillus*) were identified. Mercury methylating microbes at the family level include *Desulfobacteraceae*, *Desulfobulbaceae*, *Desulfomicrobiaceae*, *Desulfovibrionaceae*, *Syntrophaceae*, *Syntrophobacteraceae*, *Peptococcaceae*, *Ruminococcaceae*, *Syntrophomonadaceae*, *Desulfuromonadaceae*, and *Geobacteraceae* [47].

3.5. Mercury methylation, demethylation, and reduction

Significantly higher K_m, K_d, and K_v rate constants were observed in the live treatments (control, urea, NH_4Cl, and $NaNO_3$ treatments) than in the autoclaved treatment during incubation, suggesting that the methylation, demethylation, and reduction of spiked Hg tracers were biotic processes ($p < 0.05$, Fig. 3 and Fig. 4). In addition, higher K_m, K_d, and K_v values of the spiked Hg tracers were observed in all treatments (except the autoclaved treatment) during the early period of incubation ($p < 0.05$, Fig. 3 and Fig. 4). This is consistent with the findings of our previous study [39].

Nitrate addition ($NaNO_3$ treatment) significantly decreased the K_m-$^{200}Hg^{II}$ value at all sites when compared with the control treatment ($p < 0.05$, Fig. 3a-c), and this inhibition continued throughout the entire incubation period at sites GX and SK ($p < 0.05$, Figs. 3b and 3c). However, lower K_m-$^{200}Hg^{II}$ values in the $NaNO_3$ treatment compared to the control treatment were observed only during the first 16 h at site HX (Fig. 3a). At site SK, the K_m-$^{200}Hg^{II}$ value in the NH_4Cl treatment was significantly higher than that in the control treatment during incubation ($p < 0.05$, Fig. 3c). Discernable methylation of the spiked $^{202}Hg^0$ tracer was limited at sites HX and SK and was absent at site GX. Similar to the distribution pattern of K_m-$^{200}Hg^{II}$, lower K_m-$^{202}Hg^0$ values at site HX were found in the $NaNO_3$ treatment than in the control treatment ($p < 0.05$, Fig. 3g). It should be noted that some high K_m-$^{200}Hg^{II}$ and K_m-$^{202}Hg^0$ values were observed in the autoclaved samples (Figs. 3a and 3g), implying recovered microbial growth. In our parallel work, a spread-plate experiment was conducted using autoclaved samples to check the activity of microbes [38]. However, no countable colony-forming units were identified. Uncertainties in autoclaving sterilization have been reported previously, which is consistent with the current observations [77,83]. In terms of demethylation, NO_3^- input decreased the K_d-Me^{198}Hg value throughout the entire incubation period at all sites, with the only exception being the 4th hour at site GX ($p < 0.05$, Figs. 3d-3f). The K_d-Me^{198}Hg values in the control, urea, and NH_4Cl treatments were comparable for most periods at all sites. The concentrations of methylated $^{200}Hg^{II}$ and $^{202}Hg^0$ or remaining Me^{198}Hg, as well as the transformation rates of Hg isotopic tracers, are shown in Fig. S11 and Fig. S12.

Urea addition significantly increased both K_v-$^{200}Hg^{II}$ and K_v-Me^{198}Hg when compared with the control treatment for some periods (after 14 h for sites HX and GX and at the 50th h for site SK, $p < 0.05$, Fig. 4) during incubation. Similarly, masses of purgeable $^{198}Hg^0$, $^{200}Hg^0$, and $^{202}Hg^0$ from spiked tracers (Me^{198}Hg, $^{200}Hg^{II}$, and $^{202}Hg^0$) were also stimulated by urea addition ($p < 0.05$, Fig. S13). Hg reduction promoted by urea addition varied across the incubation period at each site. Specifically, significant differences in purgeable Hg^0 between the urea and control treatments were observed between the 14th-50th hour at site HX ($p < 0.05$, Fig. S13 a, d, and g), between the 14th-26th hour at site GX ($p < 0.05$, Fig. S13 b, e, and h), and only at the 50th hour at site SK ($p < 0.05$, Fig. S13 c, f, and i). There were no significant differences in the K_v-$^{200}Hg^{II}$ and K_v-Me^{198}Hg values between the control and NH_4Cl

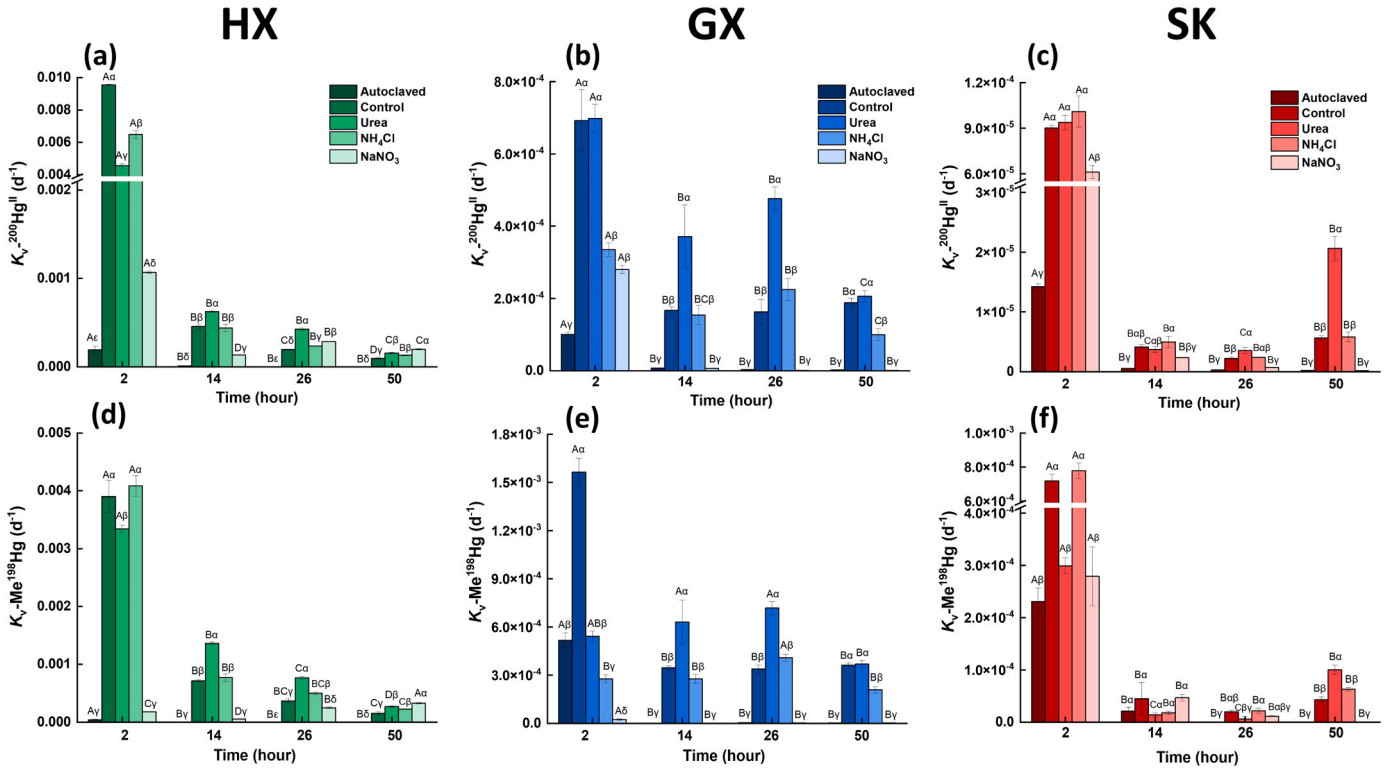

Fig. 4. Volatilization rate constants (K_v-$^{200}Hg^{II}$ in plots a, b, and c; K_v-Me^{198}Hg in plots d, e, and f) as a function of time at the three sites (HX, GX, and SK) for the different treatments. The definitions of the symbols are the same as in Fig. 3. The masses of purgeable $^{198}Hg^0$, $^{200}Hg^0$, and $^{202}Hg^0$ are shown in Fig. S13. Data for the autoclaved and control treatments were obtained from our parallel work [38].

treatments during the incubation period, but higher masses of purgeable $^{200}Hg^0$, $^{198}Hg^0$, and $^{202}Hg^0$ were observed in the NH_4Cl treatment compared to the control treatment for some times during incubation at sites HX and SK (e.g., the 26th hour at site HX and the 50th hour at site SK, $p < 0.05$, Fig. S13). Lower K_v-$^{200}Hg^{II}$ and K_v-$Me^{198}Hg$ values were observed in the $NaNO_3$ treatment than in the control treatment throughout the entire incubation period at sites GX and SK ($p < 0.05$, Fig. 4). At site HX, the K_v-$^{200}Hg^{II}$ and K_v-$Me^{198}Hg$ values were significantly lower in the $NaNO_3$ treatment than in the control treatment during the earlier period of incubation (before the 14th hour for K_v-$^{200}Hg^{II}$ and before the 28th hour for K_v-$Me^{198}Hg$) ($p < 0.05$, Figs. 4a and 4d). The transformation rates of $^{200}Hg^0$ and $^{198}Hg^0$ (ratio of purgeable Hg^0 to spiked Hg tracers) are shown in Fig. S14.

4. Discussion

4.1. N cycling and its influence on the redox of S and Fe

Dissimilatory nitrate reduction processes are the major route of N cycling in paddy slurries, where denitrification is the predominant pathway. The *narG* gene, a nitrate reductase, is involved in both the denitrification and DNRA processes, whereas the *nirS* gene, a nitrite reductase, is only involved in denitrification [35]. The significant correlations between copies of the *narG* and *nirS* genes (Fig. S5a) support the predominance of the denitrification pathway of nitrate reduction. In addition, a greater abundance of denitrifiers than community-mediated DNRA was observed at all sites ($p < 0.05$, Fig. S16). Together, these findings suggest that denitrification is likely the major pathway for the dissimilatory nitrate reduction process (Fig. 5). In addition, NH_4Cl addition acidified the soil by approximately 0.1 units of pH ($p < 0.05$, Fig. S16). More discussion related to N cycling in paddy slurries is provided in Text S4.

Sulfate reduction was inhibited in paddy slurries under nitrate addition. The higher concentrations of SO_4^{2-} in the autoclaved treatment than in the control and ammonium treatments at all sites ($p < 0.05$, Fig. S7 and S8) suggest the presence of microbially mediated sulfate reduction. However, NO_3^- addition significantly increased the concentration of SO_4^{2-} compared with the ammonium treatment (Fig. S7). In the absence of exogenous sulfate input, the high SO_4^{2-} concentration implies that the reduction in SO_4^{2-} was inhibited (Fig. 5). NO_3^- is an electron acceptor that can be used by a large number of microorganisms, and NO_3^- reduction usually outcompetes SO_4^{2-} reduction [8,21]. In addition, nitrate reducers not only compete for electrons with SRB but may also impact the survival of SRB. He et al. [21] reported the presence of nitrate stress in SRB, and this was linked to components of both osmotic and nitrite stress. Our previous work also demonstrated that NO_3^- significantly affected the microbial community composition of paddy soils [58]. The redox ladder determined by thermodynamics indicates that the reduction potential of NO_3^- is higher than that of Fe^{3+}, followed by SO_4^{2-} [5,28]. Although SO_4^{2-} reduction was inhibited in the $NaNO_3$ treatment, Fe^{3+} reduction was still in progress, which was evidenced by the increase in Fe^{2+} during incubation (Fig. S7) and the correlation between NH_4^+ and Fe^{2+} ($r = 0.44$, $p < 0.01$). This implies that Fe-reducing bacteria-mediated Hg methylation was not influenced by N addition.

4.2. Different N species-regulated Hg methylation and demethylation

Methylation of $^{200}Hg^{II}$ was suppressed by nitrate addition in paddy slurries. Nitrate addition significantly lowered the K_m-$^{200}Hg^{II}$ value (Fig. 3) and the formation of $Me^{200}Hg$ (Fig. S11) at all sites. The negative correlations between $[Me^{200}Hg]$ and $[SO_4^{2-}]$ ($r = -0.32$, $p < 0.05$ at site HX; $r = -0.48$, $p < 0.01$ at site GX; $r = -0.77$, $p < 0.01$ at site SK) imply that the inhibited $^{200}Hg^{II}$ methylation can be attributed to the hampered SO_4^{2-} reduction. In particular, SRB are major Hg methylators in the studied paddy fields [83]. Many studies conducted in aquatic systems have demonstrated that NO_3^- reduction diverts carbon and energy flows from SRB, thus suppressing Hg methylation [13,50,65,68,76]. Accordingly, the application of nitrate has been employed as a remediation approach to mitigate MeHg accumulation in aquatic biota [50,76]. However, the inhibition of SO_4^{2-} reduction from NO_3^- addition is time-dependent at different sites. For example, when SO_4^{2-} reduction commenced at site HX (after the 4th hour, Fig. S7a), inhibition of $^{200}Hg^{II}$ methylation vanished (Fig. 3a). This suggests that $^{200}Hg^{II}$ may have been methylated when SO_4^{2-} reduction mediated by SRB was refunctionalized. This finding highlights that competition from NO_3^- reduction, instead of the availability of SO_4^{2-}, is the limiting factor in sulfate reduction and SRB-mediated Hg^{II} methylation. A lower abundance of potential SRB methylators (identified by Ma et al. [47]) was observed in the $NaNO_3$ treatment than in the control treatment at all sites ($p < 0.05$, Table S4), further supporting this assertion. In addition, the higher soil organic matter (SOM) content at site HX than at sites GX and SK (Fig. S17a) may provide more electron donors to consume the added NO_3^-, which explains the recovery of SO_4^{2-} reduction during the late period of incubation (Fig. S7a). In addition to the SOM content, the concentration and composition of dissolved organic matter (DOM) are also important factors influencing the transformation of Hg in paddy fields [1,38,92]. In our parallel work, we found that DOM with a higher humification degree inhibits Hg^{II} methylation. However, this trend is dependent on study sites but independent of different treatments for a given site [38]. In addition, some higher $Me^{200}Hg$ concentrations were observed in the NH_4Cl treatment than in the control at site SK ($p < 0.05$,

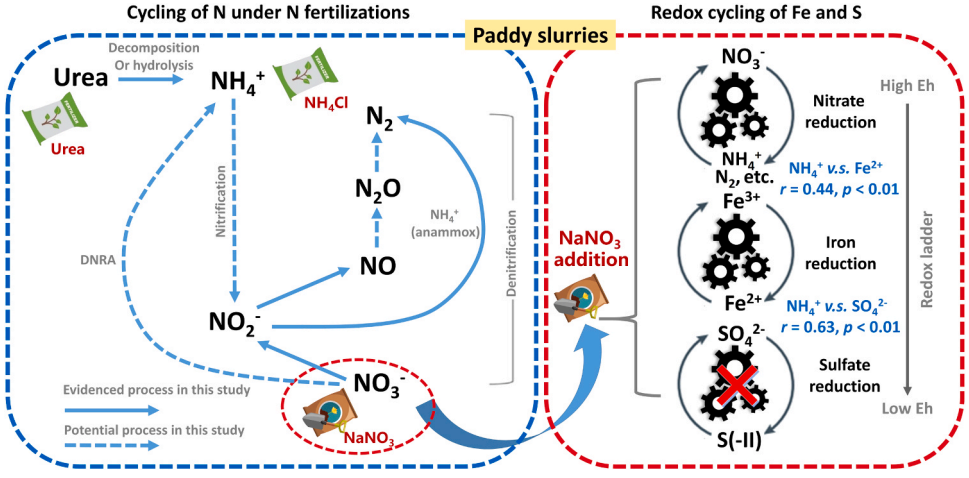

Fig. 5. Schematic diagram of N cycling and the influences of N fertilization on the redox of Fe and S in paddy slurries.

Fig. S11). This can be explained by the decreased pH in the NH_4Cl treatment (Fig. S17b), which potentially increased the bioavailability of Hg.

Demethylation of $Me^{198}Hg$ was also inhibited by nitrate addition in paddy slurries. Todorova et al. [76] suggested that nitrate regulates MeHg accumulation by (i) reducing MeHg production and (ii) promoting MeHg demethylation. The first mechanism is supported by our data, as discussed above. In terms of the second mechanism, researchers have reported that nitrate promotes the photodegradation of MeHg by forming MeHg scavengers (e.g., hydroxyl radicals) in the presence of light [20,69,87]. Here, we propose a different scenario in which nitrate addition inhibits MeHg demethylation under dark conditions. First, demethylation of the $Me^{198}Hg$ tracer was a microbially mediated process due to the lower $Me^{198}Hg$ loss ($p < 0.05$, Fig. S11) and lower K_d-$Me^{198}Hg$ value ($p < 0.05$, Fig. 3) in the autoclaved treatment compared to the other treatments. In our parallel study, we found that oxidative demethylation (OD) rather than reductive demethylation (RD) played a dominant role in MeHg degradation in flooded paddy soils under dark conditions [38]. Furthermore, SRB ($SO_4^{2-} + CH_3Hg^+ + 3\ H^+ = H_2S + CO_2 + Hg^{2+} + 2\ H_2O$) and methanogens ($4CH_3Hg^+ + 2\ H_2O + 4\ H^+ = 3CH_4 + CO_2 + 4Hg^{2+} + 4\ H_2$) are key players in OD [29,36]. Methanogenesis requires lower Eh than SO_4^{2-} reduction [5,28]. Therefore, methanogenesis could also be inhibited since SO_4^{2-} reduction was suppressed by nitrate addition. Significant inhibition of CH_4 production from NO_3^- addition was also reported by Chidthaisong and Conrad [9], Wang et al. [80] and Sriphirom et al. [66] in paddy fields. Accordingly, SRB- or methanogen-mediated $Me^{198}Hg$ demethylation was likely inhibited in the $NaNO_3$ treatment at all sites. Positive correlations between [$Me^{198}Hg$] and [SO_4^{2-}] ($r = 0.42$, $p < 0.01$ at site HX; $r = 0.52$, $p < 0.01$ at site GX; and $r = 0.59$, $p < 0.01$ at site SK) or [NO_3^-] ($r = 0.36$, $p < 0.05$ at site GX) further suggest redox-regulated MeHg demethylation. Similar findings were reported by Marvin-DiPasquale and Oremland [49] in Everglades peat sediments. Our findings offer new insights into nitrate-regulated MeHg accumulation, suggesting that nitrate is capable of inhibiting MeHg demethylation through competition for electron donors with other demethylators under dark conditions.

4.3. Different N species-regulated Hg reduction

The formation of purgeable $^{198}Hg^0$, $^{200}Hg^0$, and $^{202}Hg^0$ was inhibited by nitrate addition in paddy slurries. Similar to our parallel study [38], the amount of purgeable $^{200}Hg^0$ was significantly correlated with the amounts of purgeable $^{198}Hg^0$ and $^{202}Hg^0$ in this study (Fig. S16). This implies that the formation of purgeable $^{198}Hg^0$, $^{200}Hg^0$, and $^{202}Hg^0$ was dominated by similar mechanisms. Our previous study attributed the formation of purgeable $^{198}Hg^0$ to oxidative demethylation of $Me^{198}Hg$ and the reduction of $^{198}Hg^{II}$ and formation of purgeable $^{202}Hg^0$ to rapid abiotic oxidation of $^{202}Hg^0$ and biotic re-reduction of $^{202}Hg^{II}$ [38]. Accordingly, microbially mediated Hg^{II} reduction is a prerequisite process for the formation of purgeable $^iHg^0$ ($i = 198$, 200, and 202). Currently, dark reduction of Hg^{II} includes two pathways: (i) Hg^{II} reduction by Hg-resistant microorganisms (mediated by the *mer* operon) and (ii) Hg^{II} reduction by dissimilatory metal-reducing bacteria (DMRB) [82] and fermentation [18]. In this study, the *merA* gene (mercuric reductase) was below the detection limit, suggesting that DMRB or fermentation-mediated Hg^{II} reduction played a key role. It is known that both DMRB and fermentation transfer electrons to the outer membrane, and Hg^{II} could be a terminal electron acceptor [82]. Therefore, the availability of other extracellular electron acceptors (e.g., NO_3^- and Fe^{3+}) determines Hg^{II} reduction. As a result, the addition of NO_3^- significantly inhibited Hg^{II} reduction in paddy slurries.

The formation of purgeable $^{198}Hg^0$, $^{200}Hg^0$, and $^{202}Hg^0$ was partially facilitated by urea and NH_4Cl addition in some incubated paddy slurries. The expected behaviors of the added ammonium (i.e., both urea and NH_4Cl) in our incubation studies included four aspects: (i) volatilization, (ii) assimilation by microbes, (iii) nitrification or ammonium oxidation, and (iv) anammox [30,35]. Volatilization is unlikely to be the predominant process due to the significant differences in Hg reduction between the control and ammonium treatments, but it may explain the higher NH_4^+ concentrations in the urea treatment than in the NH_4Cl treatment at all sites ($p < 0.01$, Fig. S3). To date, no study has confirmed the links between nitrification and Hg^{II} reduction, and the role of microbial NH_4^+ assimilation in Hg cycling is still unknown. Although there is very limited experimental evidence, the utilization of NH_4^+ by Hg^{II} reducers and Hg^{II} methylators is assumed to be comparable; in particular, the Hg^{II} reducers, identified above, likely occupy a niche similar to that of methylators [18]. However, NH_4^+-promoted Hg^{II} methylation was absent at sites HX and GX (Fig. S11), suggesting that the enhanced Hg^{II} reduction did not result from the nutrient (i.e., NH_4^+) supply for Hg^{II} reducers. Anammox is an important process in N cycling [64]; it can contribute to 31–41% of N_2 production in the rhizosphere of paddy soils [55], and the total loss of N, which is linked to anammox, can reach 2.50×10^6 Mg N per year in southern China [86]. Previous studies have reported that the reduction of metal(loid)s can be coupled with anammox, e.g., iron reduction (Feammox) [12,2,72,85], manganese reduction (Mnammox) [46], and arsenic reduction (Asammox) [91]. Based on the products of metal(loid) reduction-coupled anammox (i.e., N_2, NO_2^-, and NO_3^-), we speculate that Hg^{II} reduction coupled with anammox (Hgammox) may occur as follows:

$$2NH_4^+ + 3Hg^{2+} = N_2 + 3Hg^0 + 8\ H^+\ \Delta G_f^0 = -170{\cdot}06\ \text{kJmol}^{-1} \quad (1)$$

$$NH_4^+ + 3Hg^{2+} + 2\ H_2O = NO_2^- + 3Hg^0 + 8\ H^+\ \Delta G_f^0 = 23{\cdot}33\ \text{kJmol}^{-1} \quad (2)$$

$$NH_4^+ + 4Hg^{2+} + 3\ H_2O = NO_3^- + 4Hg^0 + 10\ H^+\ \Delta G_f^0 = 22{\cdot}01\ \text{kJmol}^{-1} \quad (3)$$

By calculating the delta free energy for the above equations (Text S5), it can be seen that Eq. 1 is thermodynamically favorable with a ΔG_f^0 of -170.06 kJ mol^{-1}. This is consistent with Feammox, in which the formation of N_2 is energetically more favorable than the formation of NO_2^- and NO_3^- [79]. It has been reported that anammox-coupled metal reduction depends on the bioaccessability of metals [6,85], and Hg^{II} can strongly bind with urease [57]. Therefore, a higher bioaccessability of Hg^{II} by urea than that of NH_4Cl is expected through urease-mediated urea hydrolysis. This potentially explained the greater Hg^{II} reduction in the urea treatment than in the NH_4Cl treatment. In addition, our previous work suggests that the Fe (oxyhydr)oxide-OM association is a sink for newly added/deposited Hg in paddy soils [40]. As a result, Feammox-induced Fe (oxyhydr)oxide reduction may release Hg^{II} that could be involved in Hgammox. In addition, Sun et al. [70] documented that urea addition increased the bioavailability of Hg by enhancing the release of root exudates, which may be another reason explaining the promoted Hg^{II} reduction. Accordingly, theoretical Hgammox by the formation of N_2 and Hg^0 could occur in paddy slurries. However, more work is required to verify this hypothesis and identify the microorganisms that mediate Hgammox. Another possible reason is the imbalanced C/N/S stoichiometry due to N addition, which likely reshaped the community structures of Hg transformation-involved microbes [32]. In addition, other electron donors (e.g., HS^-, Fe^{2+}, and FeS) could also result in Hg^{II} reduction without being directly coupled to NH_4^+ oxidation [4,7].

5. Conclusions and implications

Our findings showed that different N fertilizations significantly regulated Hg methylation, demethylation and reduction processes in paddy slurries. Both methylation (Hg^{II}) and demethylation (MeHg) of Hg were constrained by nitrate addition through the inhibition of methylators (i.e., SRB) and demethylators (i.e., SRB or methanogens). Competition between nitrate reducers and SRB or methanogens was the mechanism. The reduction of Hg^{II} was inhibited because nitrate outcompeted Hg^{II} for extracellular electrons. Ammonium addition-

promoted Hg^{II} reduction deserves more work, and anammox coupled with Hg^{II} reduction may provide new insight into microbially mediated Hg^{II} reduction under dark conditions in paddy slurries. However, all the findings reported in this study were obtained through an incubation experiment with a limited incubation time, and long-term in situ field work in the presence of rice plants is also needed.

In aquatic systems, nitrate is applied to inhibit the formation of MeHg and its accumulation in food webs [13,50,76]. Similarly, Zhang et al. [94] applied nitrate to paddy soils, which resulted in reduced MeHg in rice grains. Here, we revealed two contrasting effects of nitrate on net MeHg accumulation: (i) a reduction in MeHg via the inhibition of Hg^{II} methylation ("positive effect") and (ii) the preservation of MeHg via the inhibition of MeHg demethylation under dark conditions ("negative effect"). The "positive effect" can be counteracted and even overtaken by the "negative effect", which may result in more net MeHg accumulation in nitrate treatments with an increasing incubation period. Such a finding raises questions regarding the approach to reducing MeHg accumulation by changing the redox condition, although photochemistry was not considered here. Decreases in net MeHg accumulation in the urea treatment at all sites can likely be attributed to the promotion of Hg reduction, suggesting that Hg reduction is still a useful detoxification mechanism for reducing the formation of MeHg, even though Hg^0 was also found to be a substrate of methylation [11,25]. This implies that long-term urea fertilization will reduce the MeHg burden in flooded paddy fields but will increase the Hg pool in the atmosphere. In addition, the MeHg degradation resistance of paddy slurry should be considered. Previously, MeHg was considered a labile Hg species that could be degraded or adsorbed by rice roots in paddy systems. Recently, Baptista-Salazar et al. [3] reported the formation of refractory MeHg pools in sediments and speculated that organic matter and minerals protect MeHg from degradation. However, the mechanisms underlying the stability of MeHg in flooded paddy soils should be further investigated; for example, redox-induced selective processes by microorganisms may be another factor to consider.

CRediT authorship contribution statement

Ji Chen: Methodology, Investigation, Data curation; Writing – review & editing; **Gongren Hu**: Supervision, Writing – review & editing; **Jiang Liu:** Methodology; Visualization, Formal analysis, Writing – original draft; **Alexandre J. Poulain**: Conceptualization, Writing – review & editing; **Qiang Pu**: Methodology, Writing – review & editing; **Rong Huang**: Visualization, Writing – review & editing; **Bo Meng**: Conceptualization, Methodology, Supervision, Project administration, Funding acquisition, Writing – review & editing; **Xinbin Feng**: Conceptualization, Resources, Funding acquisition, Writing – review & editing.

Declaration of Competing Interest

The authors declare that they have no known competing financial interests or personal relationships that could have appeared to influence the work reported in this paper.

Data Availability

Data will be made available on request.

Acknowledgments

This research was supported by the National Natural Science Foundation of China [grant numbers 42022024, 41931297, and 42107442], the CAS "Light of West China" program, Guizhou Provincial Natural Science Foundation [grant number Qian- Ke-He-Ji-Chu ZK [2023] Yi ban 474], and the Opening Fund of the State Key Laboratory of Environmental Geochemistry [grant number SKLEG2022201]. We thank Zhengdong Hao for his help in sample analysis. We thank Leiming Zhang for his edits and comments on the draft of this manuscript.

Appendix A. Supporting information

Supplementary data associated with this article can be found in the online version at doi:10.1016/j.jhazmat.2023.132457.

References

[1] Abdelhafiz, M.A., Liu, J., Jiang, T., Pu, Q., Wajahat, M., Zhang, K., et al., 2023. DOM influences Hg methylation in paddy soils across a Hg contamination gradient. Environ Pollut 322, 121237.
[2] Bao, P., Li, G.X., 2017. Sulfur-driven iron reduction coupled to anaerobic ammonium oxidation. Environ Sci Technol 51, 6691–6698.
[3] Baptista-Salazar, C., Liem-Nguyen, V., Jonsson, S., 2022. Experiments revealing the formation of refractory methylmercury pools in natural sediments and soils. Geochim Cosmochim Acta 328, 76–84.
[4] Bone, S.E., Bargar, J.R., Sposito, G., 2014. Mackinawite (FeS) reduces mercury(II) under sulfidic conditions. Environ Sci Technol 48, 10681–10689.
[5] Borch, T., Kretzschmar, R., Skappler, A., Van Cappellen, P., Ginder-Vogel, M., Voegelin, A., et al., 2010. Biogeochemical redox processes and their impact on contaminant dynamics. Environ Sci Technol 44, 15–23.
[6] Bosch, J., Heister, K., Hofmann, T., Meckenstock, R.U., 2010. Nanosized iron oxide colloids strongly enhance microbial iron reduction. Appl Environ Microbiol 76, 184–189.
[7] Bouffard, A., Amyot, M., 2009. Importance of elemental mercury in lake sediments. Chemosphere 74, 1098–1103.
[8] Callbeck, C.M., Agrawal, A., Voordouw, G., 2013. Acetate production from oil under sulfate-reducing conditions in bioreactors injected with sulfate and nitrate. Appl Environ Microbiol 79, 5059–5068.
[9] Chidthaisong, A., Conrad, R., 2000. Turnover of glucose and acetate coupled to reduction of nitrate, ferric iron and sulfate and to methanogenesis in anoxic rice field soil. FEMS Microbiol Ecol 31, 73–86.
[10] Clarkson, T.W., 1993. Mercury - major issues in environmental-health. Environ Health Perspect 100, 31–38.
[11] Colombo, M.J., Ha, J., Reinfelder, J.R., Barkay, T., Yee, N., 2013. Anaerobic Oxidation of Hg(0) and Methylmercury Formation by *Desulfovibrio desulfuricans* ND132. Geochim Cosmochim Acta 112, 166–177.
[12] Ding, L.J., An, X.L., Li, S., Zhang, G.L., Zhu, Y.G., 2014. Nitrogen loss through anaerobic ammonium oxidation coupled to iron reduction from paddy soils in a chronosequence. Environ Sci Technol 48, 10641–10647.
[13] Effler, S.W., Matthews, D.A., 2008. Implications of redox processes for the rehabilitation of an Urban Lake, Onondaga Lake, New York. Lake Reserv Manag 24 (2), 122–138.
[14] Feng, X., Li, P., Qiu, G., Wang, S., Li, G., Shang, L., et al., 2008. Human exposure to methylmercury through rice intake in mercury mining areas, Guizhou Province, China. Environ Sci Technol 42, 326–332.
[15] Food and Agriculture Organization of the United Nations, 2023. Fertilizers by Product, FAOSTAT. ⟨https://www.fao.org/faostat/en/#data/RFB⟩.
[16] Gilmour, C.C., Riedel, G.S., Ederington, M.C., Bell, J.T., Benoit, J.M., Gill, G.A., et al., 1998. Methylmercury concentrations and production rates across a trophic gradient in the Northern Everglades. Biogeochemistry 40, 327–345.
[17] Gray, J.E., Hines, M.E., Goldstein, H.L., Reynolds, R.L., 2014. Mercury deposition and methylmercury formation in Narraguinnep Reservoir, southwestern Colorado, USA. Appl. Geochemistry 50, 82–90.
[18] Grégoire, D.S., Poulain, A.J., 2018. Shining light on recent advances in microbial mercury cycling. Facets 3, 858–879.
[19] Gruber, N., Galloway, J.N., 2008. An earth-system perspective of the global nitrogen cycle. Nature 451, 10–13.
[20] Han, X., Li, Y., Li, D., Liu, C., 2017. Role of free radicals/reactive oxygen species in mehg photodegradation: importance of utilizing appropriate scavengers. Environ Sci Technol 51, 3784–3793.
[21] He, Q., He, Z., Joyner, D.C., Joachimiak, M., Price, M.N., Yang, Z.K., et al., 2010. Impact of elevated nitrate on sulfate-reducing bacteria: a comparative study of desulfovibrio vulgaris. ISME J 4, 1386–1397.
[22] Helmrich, S., Vlassopoulos, D., Alpers, C.N., O'Day, P.A., 2022. Critical review of mercury methylation and methylmercury demethylation rate constants in aquatic sediments for biogeochemical modeling. Crit Rev Environ Sci Technol 52, 4353–4378.
[23] Hintelmann, H., Evans, R.D., Villeneuve, J.Y., 1995. Measurement of mercury methylation in sediments by using enriched stable mercury isotopes combined with methylmercury determination by gas chromatography-inductively coupled plasma mass spectrometry. J Anal Spectrom 10, 619–624.
[24] Hintelmann, H., Keppel-Jones, K., Evans, R.D., 2000. Constants of mercury methylation and demethylation rates in sediments and comparison of tracer and ambient mercury availability. Environ Toxicol Chem 19, 2204–2211.
[25] Hu, H., Lin, H., Zheng, W., Tomanicek, S.J., Johs, A., Feng, X., et al., 2013. Oxidation and methylation of dissolved elemental mercury by anaerobic bacteria. Nat Geosci 6, 751–754.
[26] Ishii, S., Ikeda, S., Agriculture, N., Minamisawa, K., 2011. Minireview nitrogen cycling in rice paddy environments: past achievements and future challenges. Microbes Environ 26, 282–292.

[27] Jonsson, S., Skyllberg, U., Nilsson, M.B., Westlund, P., Shchukarev, A., Lundberg, E., et al., 2012. Mercury methylation rates for geochemically relevant Hg^{II} species in sediments. Environ Sci Technol 46, 11653–11659.

[28] Kögel-Knabner, I., Amelung, W., Cao, Z., Fiedler, S., Frenzel, P., Jahn, R., et al., 2010. Biogeochemistry of paddy soils. Geoderma 157, 1–14.

[29] Kronberg, R.M., Schaefer, J.K., Bjorn, E., Skyllberg, U., 2018. Mechanisms of methyl mercury net degradation in alder swamps: the role of methanogens and abiotic processes. Environ Sci Technol Lett 5, 220–225.

[30] Kuypers, M.M.M., Marchant, H.K., Kartal, B., 2018. The microbial nitrogen-cycling network. Nat Rev Microbiol 16, 263–276.

[31] Kwon, S.Y., Selin, N.E., Giang, A., Karplus, V.J., Zhang, D., 2018. Present and future mercury concentrations in chinese rice: insights from modeling. Glob Biogeochem Cycles 32, 437–462.

[32] Li, Y., Dai, S.S., Zhao, J., Hu, Z.C., Liu, Q., Feng, J., et al., 2023. Amendments of nitrogen and sulfur mitigate carbon-promoting effect on microbial mercury methylation in paddy soils. J Hazard Mater 448, 130983.

[33] Lan, T., Xie, N., Chen, C., He, X., Deng, O., Zhou, W., et al., 2022. Effects of biological nitrification inhibitor in regulating NH_3 volatilization and fertilizer nitrogen recovery efficiency in soils under rice cropping. Sci Total Environ 838, 155857.

[34] Landa, E.R., 1978. The retention of metallic mercury vapor by soils. Geochim Cosmochim Acta 42, 1407–1411.

[35] Levy-Booth, D.J., Prescott, C.E., Grayston, S.J., 2014. Microbial functional genes involved in nitrogen fixation, nitrification and denitrification in forest ecosystems. Soil Biol Biochem 75, 11–25.

[36] Lin, C.C., Yee, N., Barkay, T., 2012. Microbial transformations in the mercury cycle. In: Liu, G.L., et al. (Eds.), In Environmental Chemistry and Toxicology of Mercury. Wiley, New Jersey, pp. 155–192.

[37] Linquist, B.A., Liu, L.J., van Kessel, C., van Groenigen, K.J., 2013. Enhanced efficiency nitrogen fertilizers for rice systems: meta-analysis of yield and nitrogen uptake. F Crop Res 154, 246–254.

[38] Liu, J., Chen, J., Poulain, A.J., Pu, Q., Hao, Z.D., Meng, B., et al., 2023. Mercury and sulfur redox cycling affect methylmercury levels in rice paddy soils across a contamination gradient. Environ Sci Technol 57, 8149–8160.

[39] Liu, J., Lu, B., Poulain, A.J., Zhang, R., Zhang, T., Feng, X., et al., 2022. The underappreciated role of natural organic matter bond Hg(II) and nanoparticulate HgS as substrates for methylation in paddy soils across a Hg concentration gradient. Environ Pollut 292, 118321.

[40] Liu, J., Lei, Z., Kong, K., Abdelhafiz, M.A., Tian, S., Jiang, T., et al., 2022. Uncovering the geochemical fractionation of newly deposited Hg in paddy soil using a stable isotope tracer. J Hazard Mater 433, 128752.

[41] Liu, J., Meng, B., Poulain, A.J., Meng, Q., Feng, X., 2021. Stable isotope tracers identify sources and transformations of mercury in rice (*Oryza sativa L.*) growing in a mercury mining area. Fundam Res 1, 259–268.

[42] Liu, M., Zhang, Q., Cheng, M., He, Y., Chen, L., Shen, H., et al., 2019. Rice life cycle-based global mercury biotransport and human methylmercury exposure. Nat Commun 10, 5164.

[43] Liu, Y.R., He, J.Z., Zhang, L.M., Zheng, Y.M., 2012. Effects of long-term fertilization on the diversity of bacterial mercuric reductase gene in a chinese upland soil. J Basic Microbiol 52, 35–42.

[44] Lucotte, M., Montgomery, S., Bégin, M., 1999. Mercury and methylmercury in natural ecosystems of northern québec. In: Lucotte, M., et al. (Eds.), Mercury in the Biogeochemical Cycle: Natural Environments and Hydroelectric Reservoirs of Northern Québec (Canada). Springer, Berlin, pp. 55–144.

[45] Ludemann, C.I., Gruere, A., He, P., Dobermann, A., 2022. Global data on fertilizer use by crop and by country. Sci Data 9, 501.

[46] Luther, G.W., Sundby, B., Lewis, B.L., Brendel, P.J., Silverberg, N., 1997. Interactions of manganese with the nitrogen cycle: Alternative pathways to dinitrogen. Geochim Cosmochim Acta 61, 4043–4052.

[47] Ma, M., Du, H., Wang, D., 2019. Mercury methylation by anaerobic microorganisms: a review. Crit Rev Environ Sci Technol 49, 1893–1936.

[48] Mao, Y., Li, Y., Richards, J., Cai, Y., 2013. Investigating uptake and translocation of mercury species by sawgrass (cladium jamaicense) using a stable isotope tracer technique. Environ Sci Technol 47, 9678–9684.

[49] Marvin-DiPasquale, M.C., Oremland, R.S., 1998. Bacterial methylmercury degradation in Florida Everglades peat sediment. Environ Sci Technol 32, 2556–2563.

[50] Matthews, D.A., Babcock, D.B., Nolan, J.G., Prestigiacomo, A.R., Effler, S.W., Driscoll, C.T., et al., 2013. Whole-lake nitrate addition for control of methylmercury in mercury-contaminated onondaga Lake, NY. Environ Res 125, 52–60.

[51] Meng, B., Feng, X., Qiu, G., Anderson, C.W.N., Wang, J., Zhao, L., 2014. Localization and speciation of mercury in brown rice with implications for pan-asian public health. Environ Sci Technol 48, 7974–7981.

[52] Meng, B., Feng, X., Qiu, G., Cai, Y., Wang, D., Li, P., et al., 2010. Distribution patterns of inorganic mercury and methylmercury in Tissues of Rice (*Oryza sativa L.*) plants and possible bioaccumulation pathways. J Agric Food Chem 58, 4951–4958.

[53] Meng, B., Feng, X., Qiu, G., Liang, P., Li, P., Chen, C., et al., 2011. The process of methylmercury accumulation in rice (*Oryza sativa L.*). Environ Sci Technol 45, 2711–2717.

[54] Meng, B., Li, Y., Cui, W., Jiang, P., Liu, G., Wang, Y., et al., 2018. Tracing the uptake, transport, and fate of mercury in sawgrass (*Cladium jamaicense*) in the florida everglades using a multi-isotope technique. Environ Sci Technol 52, 3384–3391.

[55] Nie, S., Li, H., Yang, X., Zhang, Z., Weng, B., Huang, F., 2015. Nitrogen loss by anaerobic oxidation of ammonium in rice rhizosphere. ISME J 9, 2059–2067.

[56] NSP-Fertilizer Specifications (Food and Agriculture Organization of the United Nations, 2022), ⟨https://www.fao.org/agriculture/crops/thematic-sitemap/theme/spi/plantnutrition/fertspecs/en/⟩.

[57] Ögren, L., Johansson, G., 1978. Determination of traces of mercury(II) by inhibition of an enzyme reactor electrode loaded with immobilized urease. Anal Chim Acta 96 (1), 1–11.

[58] Pu, Q., Zhang, K., Poulain, A.J., Liu, J., Zhang, R., Abdelhafiz, M.A., et al., 2022. Mercury drives microbial community assembly and ecosystem multifunctionality across a Hg contamination gradient in rice paddies. J Hazard Mater 435, 129055.

[59] Qiu, G., Feng, X., Li, P., Wang, S., Li, G., Shang, L., et al., 2008. Methylmercury accumulation in Rice (*Oryza sativa L.*) grown at abandoned mercury Mines in Guizhou, China. J Agric Food Chem 56, 2465–2468.

[60] Qureshi, A., O'Driscoll, N.J., Macleod, M., Neuhold, Y.M., Hungerbühler, K., 2010. Photoreactions of mercury in surface ocean water: gross reaction kinetics and possible pathways. Environ Sci Technol 44, 644–649.

[61] Qvarnström, J., Frech, W., 2002. Mercury species transformations during sample pre-treatment of biological tissues studied by HPLC-ICP-MS. J Anal Spectrom 17, 1486–1491.

[62] Rothenberg, S.E., Feng, X., 2012. Mercury cycling in a flooded rice paddy. J. Geophys. Res. Biogeosci. 117, 1–16.

[63] Shan, J., Zhao, X., Sheng, R., Xia, Y., Ti, C., Quan, X., et al., 2016. Dissimilatory nitrate reduction processes in typical chinese paddy soils: rates, relative contributions, and influencing factors. Environ Sci Technol 50, 9972–9980.

[64] Shan, J., Yang, P., Shang, X., Rahman, M.M., Yan, X., 2018. Anaerobic ammonium oxidation and denitrification in a paddy soil as affected by temperature, pH, organic carbon, and substrates. Biol Fertil Soils 54, 341–348.

[65] Shih, R., Robertson, W.D., Schiff, S.L., Rudolph, D.L., 2011. Nitrate controls methyl mercury production in a streambed bioreactor. J Environ Qual 40, 1586–1592.

[66] Sriphirom, P., Towprayoon, S., Yagi, K., Rossopa, B., Chidthaisong, A., 2022. Changes in methane production and oxidation in rice paddy soils induced by biochar addition. Appl Soil Ecol 179, 104585.

[67] Sonke, J.E., Angot, H., Zhang, Y., Poulain, A., Björn, E., Schartup, A., 2023. Global change effects on biogeochemical mercury cycling. Ambio 853–876.

[68] Strickman, R.J., Mitchell, C.P.J., 2018. Mercury methylation in stormwater retention ponds at different stages in the management lifecycle. Environ Sci Process Impacts 20, 595–606.

[69] Sun, R., Wang, D., Mao, W., Ma, M., Zhang, C., Jiang, T., 2015. Diurnal characteristics of migration and transformation of mercury and effects of nitrate in Jialing River, Chongqing, China. Chemosphere 119, 634–641.

[70] Sun, T., Xie, Q., Li, C., Huang, J., Yue, C., Zhao, X., et al., 2022. Inorganic versus organic fertilizers: how do they lead to methylmercury accumulation in rice grains. Environ Pollut 314, 120341.

[71] Sunderland, E.M., Li, M., Bullard, K., 2018. Decadal changes in the edible supply of seafood and methylmercury exposure in the united states. Environ Health Perspect 126, 017006.

[72] Tan, X., Xie, G.J., Nie, W.B., Xing, D.F., Liu, B.F., Ding, J., et al., 2022. Fe(III)-mediated anaerobic ammonium oxidation: a novel microbial nitrogen cycle pathway and potential applications. Crit Rev Environ Sci Technol 52, 2962–2994.

[73] Tang, Z., Fan, F., Deng, S., Wang, D., 2020. Mercury in rice paddy fields and how does some agricultural activities affect the translocation and transformation of mercury - a critical review. Ecotoxicol Environ Saf 202, 110950.

[74] Tang, Z., Fan, F., Wang, X., Shi, X., Deng, S., Wang, D., 2018. Mercury in rice (Oryza sativa L.) and rice-paddy soils under long-term fertilizer and organic amendment. Ecotoxicol Environ Saf 150, 116–122.

[75] Tang, Z., Fan, F., Wang, X., Shi, X., Wang, D., 2021. Understanding the effects of long-term different fertilizer applications on methylmercury accumulation in rice (Oryza sativa L.) plants. Sci Total Environ 777, 146125.

[76] Todorova, S.G., Driscoll, C.T., Matthews, D.A., Effler, S.W., Hines, M.E., Henry, E. A., 2009. Evidence for regulation of monomethyl mercury by nitrate in a seasonally stratified, Eutrophic Lake. Environ Sci Technol 43, 6572–6578.

[77] Tuominen, L., Kairesalo, T., Hartikainen, H., 1994. Comparison of methods for inhibiting bacterial activity in sediment. Appl Environ Microbiol 60, 3454–3457.

[78] United Nations Environment Programme. 2019. Global Mercury Assessment 2018, Geneva.

[79] Wan, L., Liu, H., Wang, X., 2022. Anaerobic ammonium oxidation coupled to Fe (III) reduction: discovery, mechanism and application prospects in wastewater treatment. Sci Total Environ 818, 151687.

[80] Wang, J., Xu, T., Yin, L., Han, C., Deng, H., Jiang, Y., et al., 2018. Nitrate addition inhibited methanogenesis in paddy soils under long-term managements. Plant, Soil Environ 64, 393–399.

[81] Wang, Y., Li, Y., Liu, G., Wang, D., Jiang, G., Cai, Y., 2015. Elemental mercury in natural waters: occurrence and determination of particulate Hg(0). Environ Sci Technol 49, 9742–9749.

[82] Wiatrowski, H.A., Ward, P.M., Barkay, T., 2006. Novel reduction of mercury (II) by mercury-sensitive dissimilatory metal reducing bacteria. Environ Sci Technol 40, 6690–6696.

[83] Wu, Q., Hu, H., Meng, B., Wang, B., Poulain, A.J., Zhang, H., et al., 2020. Methanogenesis is an important process in controlling MeHg concentration in rice paddy soils affected by mining activities. Environ Sci Technol 54, 13517–13526.

[84] Wu, Y., Xi, X., Tang, X., Luo, D., Gu, B., Lam, S.K., et al., 2018. Policy distortions, farm size, and the overuse of agricultural chemicals in China. Proc Natl Acad Sci USA 115, 7010–7015.

[85] Yang, W.H., Weber, K.A., Silver, W.L., 2012. Nitrogen loss from soil through anaerobic ammonium oxidation coupled to iron reduction. Nat Geosci 5, 538–541.

[86] Yang, X.R., Li, H., Nie, S.A., Su, J.Q., Weng, B., Sen, et al., 2015. Potential contribution of anammox to nitrogen loss from paddy soils in southern China. Appl Environ Microbiol 81, 938–947.
[87] Zepp, R.G., 1987. Nitrate-induced photooxidation of trace organic chemicals in water. Environ Sci Technol 21, 443–450.
[88] Zhang, L., Yin, Y., Sun, Y., Liang, X., Graham, D.E., Pierce, E.M., et al., 2023. Inhibition of methylmercury and methane formation by nitrous oxide in arctic tundra soil microcosms. Environ Sci Technol 57, 5655–5665.
[89] Zhang, H., Feng, X., Larssen, T., Qiu, G., Vogt, R.D., 2010. In Inland China, rice, rather than fish, is the major pathway for methylmercury exposure. Environ Health Perspect 118, 1183–1188.
[90] Zhang, H., Feng, X.B., Larssen, T., Shang, L.H., Li, P., 2010. Bioaccumulation of Methylmercury versus Inorganic Mercury in Rice (*Oryza sativa L.*) Grain. Environ Sci Technol 44, 4499–4504.
[91] Zhang, M., Kolton, M., Häggblom, M.M., Sun, X., Yu, K., He, B., et al., 2022. Anaerobic ammonium oxidation coupled to arsenate reduction, a novel biogeochemical process observed in arsenic-contaminated paddy soil. Geochim Cosmochim Acta 335, 11–22.
[92] Zhang, S., Wang, M., Liu, J., Tian, S., Yang, X., Xiao, G., et al., 2022. Biochar affects methylmercury production and bioaccumulation in paddy soils: insights from soil-derived dissolved organic matter. J Environ Sci 119, 68–77.
[93] Zhang, X., Davidson, E.A., Mauzerall, D.L., Searchinger, T.D., Dumas, P., Shen, Y., 2015. Managing nitrogen for sustainable development. Nature 528, 51–59.
[94] Zhang, Y., Liu, Y.R., Lei, P., Wang, Y.J., Zhong, H., 2018. Biochar and nitrate reduce risk of methylmercury in soils under straw amendment. Sci Total Environ 619–620, 384–390.
[95] Zhao, L., Anderson, C.W.N., Qiu, G., Meng, B., Wang, D., Feng, X., 2016. Mercury methylation in paddy soil: source and distribution of mercury species at a Hg Mining Area, Guizhou Province, China. Biogeosciences 13, 2429–2440.
[96] Zhao, L., Qiu, G., Anderson, C.W.N., Meng, B., Wang, D., Shang, L., et al., 2016. Mercury methylation in rice paddies and its possible controlling factors in the Hg mining area, Guizhou Province, Southwest China. Environ Pollut 215, 1–9.
[97] Zhu, G., Wang, S., Wang, Y., Wang, C., Risgaard-petersen, N., Jetten, M.S.M., et al., 2011. Anaerobic ammonia oxidation in a fertilized paddy soil. ISME J 5, 1905–1912.
[98] Zhu, W., Song, Y., Adediran, G.A., Jiang, T., Reis, A.T., Pereira, E., et al., 2018. Mercury transformations in resuspended contaminated sediment controlled by redox conditions, chemical speciation and sources of organic matter. Geochim Cosmochim Acta 220, 158–179.